Appl. Phys. B (2014) 117:279–286
DOI 10.1007/s00340-014-5832-z

Applied Physics B
Lasers and Optics

Reducing the line curvature error of mechanically ruled gratings by interferometric control

Haili Yu · Xiaotian Li · Jiwei Zhu · Hongzhu Yu · Xiangdong Qi · Shulong Feng

Received: 15 January 2014 / Accepted: 31 March 2014 / Published online: 22 April 2014

Abstract Line curvature error greatly influences the quality of the diffraction wave fronts of machine-ruling gratings. To reduce the line curvature error, we propose a correction method that uses interferometric control. This method uses diffraction wave fronts of symmetrical orders to compute the mean line curvature error of the ruled grating, taking the mean line curvature error as the system line curvature error. To minimize the line curvature error of the grating, a dual-frequency laser interferometer is used as a real-time position feedback for the grating ruling stage, along with using a piezoelectric actuator to adjust the stage positioning to compensate the line curvature error. Our experiments show that the proposed method effectively reduced the peak-to-valley value of the line curvature error, improving the quality of the grating diffraction wave front.

1 Introduction

Plane diffraction gratings [1]—which have excellent optical functions such as polychromatic light dispersion, polarization, and phase matching—are very popular for military, astronomy, defense, and civilian applications, among others [2–4]. These gratings are mainly produced by mechanical ruling [2] and ion-beam etching [5]. Until now, mechanical ruling has been the main way to produce echelles [6] and infrared-laser gratings, which require deep grooves with strict shapes.

In mechanical ruling, a variety of issues can produce nonideal curved gratings, including overly flexible and straightless errors of ruling carriage guides, and other errors in the ruling system [7–12], leading to line curvature error [13], which influences the peak-to-valley value and quality of the grating diffraction wave front. When the ruling system of a grating ruling machine performs consistently, the shape and amplitude of the line curvature error will remain nearly the same under the same ruling conditions. Using an interferometer to measure the wave front, Harrison et al. [14] measured the curvature of a grating ruled by an MIT-C machine, a large grating ruling machine with the highest precision in the world. The result shows that the grating ruled by the MIT-C still had a large enough line curvature error to influence the diffraction wave front of the grating produced by it. Researchers at Changchun Institute of Optics, Fine Mechanics and Physics in China are studying how to rule large gratings and have found that line curvature error is one of the most important influencers of the quality of the diffraction wave front of plane gratings [15, 16].

Line curvature error can be reduced by changing the mechanical structure of the ruling system. For example, Harrison et al. [14] found that the diamond tool guide of the MIT-C bent too much during their experiments, so they changed the section of the guide from 1.25 × 2.5 into 3.75 × 4 in. However, comparing many different mechanical structures to find the best choice is time-consuming and inefficient. In this article, we propose a correction method using interferometric control, including a

H. Yu (✉) · X. Li · J. Zhu · H. Yu · X. Qi · S. Feng
Grating Technology Laboratory, Changchun Institute of Optics and Fine Mechanics and Physics, Chinese Academy of Sciences, Changchun 130033, Jilin, China
e-mail: yuhailitc@163.com

H. Yu
University of Science and Technology of China, Hefei 230026, Anhui, China

H. Yu
Changchun Yuheng Optics Co., Ltd, Changchun 130012, Jilin, China

detailed mathematical model. Our method uses diffraction wave fronts of symmetrical orders [16, 17] to compute the mean line curvature error of a ruled grating, taking the mean line curvature error as the system error of the grating ruling machine. We performed experiments that used interferometric control [18, 19] during grating ruling to reduce the peak-to-valley value of the line curvature error.

2 Extracting the Line curvature error by grating diffraction wave fronts

Line curvature error is a main component of grating line error. To extract line curvature error, the grating line errors should first be extracted. We deduce the relationship among the grating line error, the substrate-surface error, and the grating diffraction wave front by using the geometrical optics method [16, 17]. We assume that parallel monochromatic light with wavelength λ is incident to the surface of the planar reflection grating with grating constant d, incident angle θ_1, and diffraction angle θ_2.

First, consider the case when the grating only has grating-surface error, as shown in Fig. 1. If the direction of the grating line is along the z axis and one point of the grating line p has surface-depth error $h(x_p, y_p, z_{pi})$, the total optical path difference δ_{bpi} of the incident light and the diffracted light caused by $h(x_p, y_p, z_{pi})$ can be written as

$$\delta_{bpi} = \delta_{b1} + \delta_{b2} = h(x_p, y_p, z_{pi})(\cos\theta_1 + \cos\theta_2). \quad (1)$$

Then, consider the case when the grating only has grating line error. If one point of the grating line p has grating line error $w(x_p, y_p, z_{pi})$ as shown in Fig. 2, the total optical path difference δ_{rpi} of the incident light and the diffracted light caused by $w(x_p, y_p, z_{pi})$ can be written as

$$\delta_{rpi} = \delta_{r1} + \delta_{r2} = w(x_p, y_p, z_{pi})(\sin\theta_1 + \sin\theta_2) \quad (2)$$

For the plane diffraction grating, the grating equation is

$$d(\sin\theta_1 + \sin\theta_2) = m\lambda \quad (3)$$

where m is grating diffraction order, d is the grating constant, and λ is grating wavelength.

By combining Eqs. (1)–(3), we get the total optical path difference δ_{pi} caused by the surface-depth error $h(x_p, y_p, z_{pi})$ and the grating line error $w(x_p, y_p, z_{pi})$:

$$\begin{aligned}\delta_{pi} &= \delta_{bpi} + \delta_{rpi} \\ &= h(x_p, y_p, z_{pi})(\cos\theta_1 + \cos\theta_2) + w(x_p, y_p, z_{pi})m\lambda/d.\end{aligned} \quad (4)$$

By using the interferometer to measure the diffraction wave front of the plane grating, the absolute values of the incidence angle θ_1 and the diffraction angle θ_2 often equal

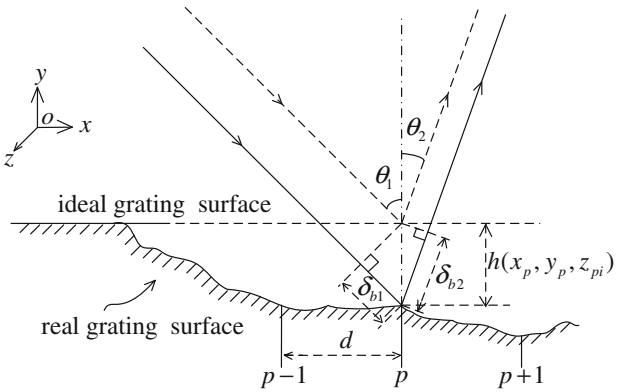

Fig. 1 Optical path difference from surface error

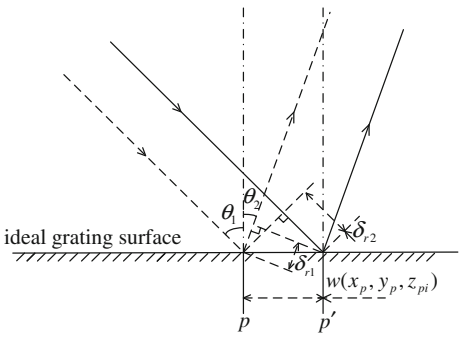

Fig. 2 Optical path difference from line error

each other [14–16]. Then, according to Eq. (4), the diffraction wave front of the grating can be written as

$$\Delta(m) = 2H\cos\theta_1 + Wm\lambda/d \quad (5)$$

where H is the substrate-surface error of the grating's entire surface, and W is the grating line error of the grating's entire surface.

If we get $\Delta(m)$ and $\Delta(-m)$, the grating diffraction wave fronts of the symmetrical diffraction orders, then the grating line error becomes

$$W = \frac{[\Delta(m) - \Delta(-m)]d}{2m\lambda}. \quad (6)$$

We assume the grating line error W calculated by Eq. (6) can be written as

$$W = \begin{bmatrix} \varepsilon_{11} & \varepsilon_{12} & \varepsilon_{13} & \cdots & \varepsilon_{1b} \\ \varepsilon_{21} & \varepsilon_{22} & \varepsilon_{23} & \cdots & \varepsilon_{2b} \\ \varepsilon_{31} & \varepsilon_{32} & \varepsilon_{33} & \cdots & \varepsilon_{3b} \\ \vdots & \vdots & \vdots & \ddots & \vdots \\ \varepsilon_{a1} & \varepsilon_{a2} & \varepsilon_{a3} & \cdots & \varepsilon_{ab} \end{bmatrix} \quad (7)$$

where each column of W is along the grating line direction.

After subtracting the yaw error and the overall position error of each grating line from Eq. (7), each element of the line curvature error B of the grating can be written as

$$b_{ij} = \varepsilon_{ij} - \frac{(\varepsilon_{aj} - \varepsilon_{1j})(i-1)}{a-1} - \varepsilon_{1j} \tag{8}$$

where $i = 1, 2, 3,\ldots,a$; $j = 1,2,3,\ldots, b$.

To obtain the mean line curvature error B_m of the grating, we average each column of matrix B in Eq. (8) and get

$$B_m = \left[\sum_{j=1}^{b} b_{1j} \sum_{j=1}^{b} b_{2j} \sum_{j=1}^{b} b_{3j} \cdots \sum_{j=1}^{b} b_{aj}\right]^T. \tag{9}$$

3 Correcting the line curvature error of plane grating by interferometrical control

To correct the line curvature error, we propose using a dual-frequency laser interferometer as a real-time position feedback for the grating ruling stage, along with using a piezoelectric actuator to adjust the stage positioning to compensate the line curvature error. The detailed steps are as follows: (a) measure the symmetrical-order diffraction wave fronts of the ruled grating and calculate the mean line curvature error B_m by Eq. (11); (b) perform least-squares curve fitting of the mean line curvature error B_m; (c) according to the mechanical structure of the grating ruling machine, calculate the relationship between the displacement of the stage and elapsed time; (d) using the dual-frequency laser interferometer, measure the real-time displacement of the stage, simultaneously adjusting the real-time displacement of the stage with a piezoelectric actuator to minimize the line curvature error. For closed-loop control of piezoelectric actuators, we use proportion integration differentiation (PID) control with parameters adjusted by a BP neural network algorithm, BP-PID.

Currently, the primary grating ruling machines in China are CIOMP-1 through CIOMP-5 at the Changchun Institute of Optics, Fine Mechanics and Physics. CIOMP-2 (see Fig. 3) has the best stage-positioning accuracy of all Chinese grating ruling machines, with a short-term stage-positioning error as low as 5 nm. In this paper, we corrected the line curvature error of CIOMP-2 [18, 19] by using interferometric control.

3.1 Overall structure of the CIOMP-2 grating ruling machine

The mechanical structure of a grating ruling machine includes the ruling system and the feeding system. The ruling system realizes the reciprocating motion of the diamond tool, and the feeding system realizes the one-directional feeding motion of the grating blank. The main components of the CIOMP-2 ruling system include the ruling motor, crank link, copper slide, copper slide guide, push–pull rod, saddle slider, ruling carriage, and fused-silica guide (see Fig. 4). Now, we will introduce the

Fig. 3 CIOMP-2 grating ruling machine

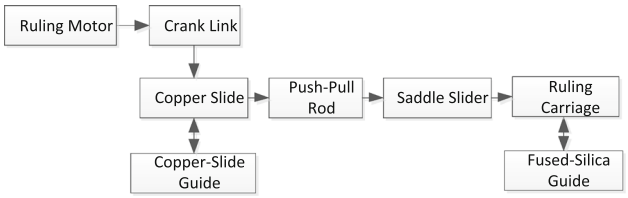

Fig. 4 Schematic of the CIOMP-2 ruling system

working principle of the CIOMP-2 ruling system: To produce the reciprocating motion of the diamond tool along the fused-silica guide, the crank link—driven by the ruling motor—moves the saddle slider across the fused-silica guide by a copper slide and push–pull rod. The ruling carriage is installed at one side of the saddle slider, and the diamond tool is at the bottom of the ruling carriage. Helped by the closure-force contact between the saddle slider and fused-silica guide, the diamond tool moves along one side of the surface of the fused-silica guide, ruling the grating blank as the saddle slider returns.

The CIOMP-2 feeding system uses a macro–micro stage, which includes a macro-positioning stage and a micro-positioning stage (see Fig. 5). The macro-positioning and micro-positioning stages are used to realize micron-scale coarse positioning and nanoscale accurate positioning of the grating blank, respectively. The macro-positioning stage has a basin-type structure, and the micro-positioning stage is embedded in the macro-positioning stage with four thin, symmetrical steel sheets (see Fig. 5). The piezoelectric actuator (PAHL 120/20; Jenoptik AG, Jena, Germany) is mounted between the macro-positioning stage and micro-positioning stage. The actuator has a displacement resolution of 0.15 nm and a maximum elongation value of 120 μm.

The principle of the CIOMP-2 feeding system (see Fig. 6) mainly includes the following two steps: First, the feeding motor slows from the gear reducer successively driving the worm gear and screw nut, allowing the macro-

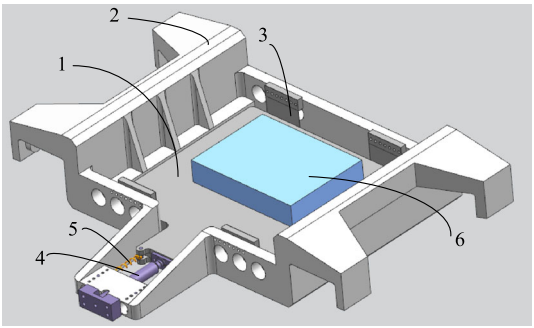

Fig. 5 Schematic of the macro–micro stage. *1* micro-positioning stage, *2* macro-positioning stage, *3* steel sheet, *4* PZT actuator, *5* tension spring, *6* grating blank

Fig. 6 Schematic of the CIOMP-2 feeding system

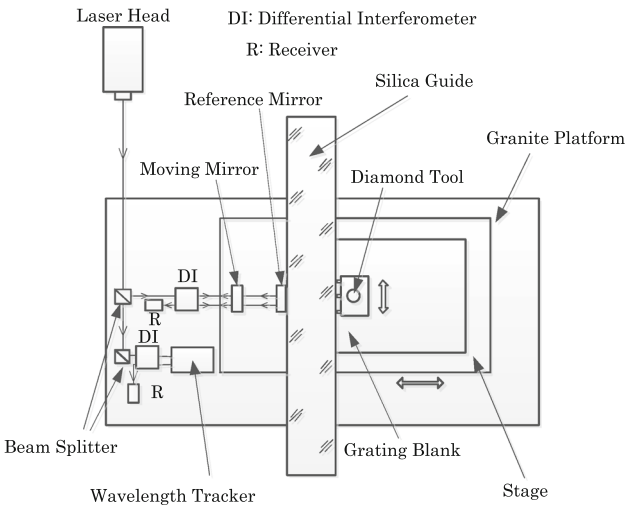

Fig. 7 Optical layout of the laser interferometer

positioning stage to perform coarse positioning. Then, according to the deviation in position between the ideal position and actual position, acquired by the dual-frequency laser interferometer, the piezoelectric actuator adjusts the accurate nanoscale positioning of the micro-positioning stage and grating blank.

3.2 Optical layout of the dual-frequency laser interferometer

Figure 7 shows the optical layout of the laser interferometer on CIOMP-2, the position resolution of which can reach as low as 0.15 nm. Two beam splitters and two differential interferometers are fixed to the granite platform. One optical

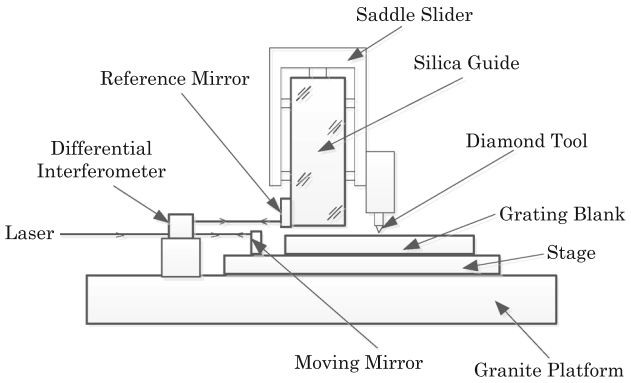

Fig. 8 Positions of the reference and measuring mirrors

path of the dual-frequency laser has a wavelength tracker, which is used to monitor the influence of the external environment (such as the refractive index of the air, the temperature, and humidity) on the real-time position-measuring accuracy of the dual-frequency laser interferometer.

Another optical path of the dual-frequency laser has a measuring mirror on the micro-positioning stage and a reference mirror on the fused-silica guide, which are used to measure the relative displacement between the micro-positioning stage and the fused-silica guide of the ruling system (see Fig. 8).

3.3 Proposed method to correct the line curvature error

As shown in Fig. 9, we assume the grating line length to be L_g and that the diamond tool rules each grating line along the direction of the grating line. For the ruling of each grating line, the diamond tool starts at point D_O and ends at point D_E. Point D_C is the current position of the diamond tool. We define the distance between the current position D_C and origin position D_O of the diamond tool as the diamond tool displacement s. Under this definition, the diamond tool displacement s is some value between 0 and the grating line length L_g.

Using least-squares method to fit Eq. (9), we get the curve fit $E(s)$ of the line curvature error, which includes the relationship between the line curvature error and the diamond tool displacement s. We assume $E(s)$ can be expressed as

$$E(s) = \sum_{q=0}^{h} c_q s^q, \quad q = 1, 2, 3, \ldots, \mathrm{h}. \tag{10}$$

To correct the line curvature error caused by the CIOMP-2 ruling system, we need to adjust the displacement of the micro-positioning stage by the opposite value of the line curvature error: $-E(s)$.

The CIOMP-2 diamond tool runs at a nonuniform speed. Before correcting the line curvature error, we must get the relationship between the diamond tool displacement s and

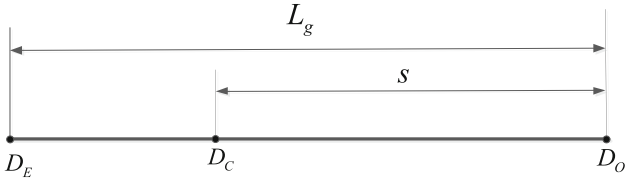

Fig. 9 Schematic of the diamond tool displacement s

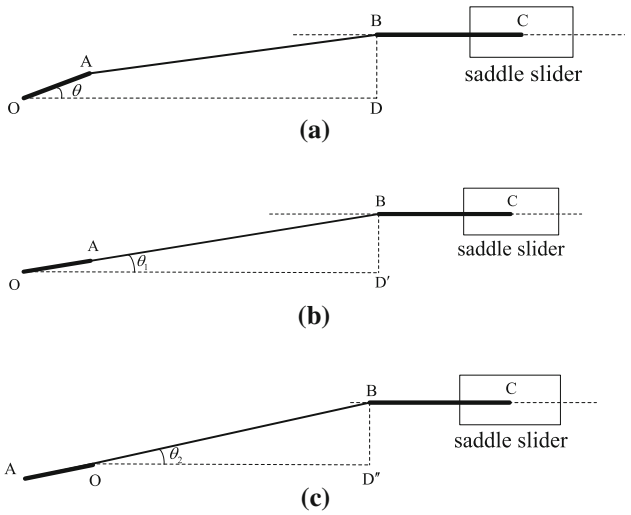

Fig. 10 Principle schematic of the crank link in various positions: **a** random position; **b** $L = L_{\max}$; **c** $L = L_{\min}$

the spent time T_s from the structure of the crank link of the ruling system. As shown in Fig. 10, we define the center of the crank as point O, the two ends of the link as points A and B, the two ends of the push–pull rod as points B and C, and the effective radius of the crank as OA. Point A is the joint point between the crank and link, point B is the joint point between the link and push–pull rod, and point C is the joint point between the push–pull rod and saddle slider. The vertical distance between the center of the crank O and the push–pull rod is BD.

In Fig. 10, $BC \| OD$, $BC \| OD'$, $BC \| OD''$, $BD \perp OD$, $BD' \perp OD'$, $BD'' \perp OD''$, $\angle AOD = \theta$, $\angle AOD' = \theta_1$, and $\angle AOD'' = \theta_2$. We assume $OA = r$, $BD = h_{BD}$, and $OD = L$. Judging from the principle of the crank link, the maximum value $L_{\max}$ of L occurs when the saddle slider is farthest from point O (see Fig. 10b), and the minimum value $L_{\min}$ of L occurs when the saddle slider is nearest to point O (see Fig. 10c). According to Fig. 10, we get

$$\begin{cases} L = r\cos\theta + \sqrt{L_{AB}^2 - (h_{BD} - r\sin\theta)^2} \\ L_{\max} = \sqrt{(L_{AB} + r)^2 - h_{BD}^2} \\ L_{\min} = \sqrt{(L_{AB} - r)^2 - h_{BD}^2} \\ L_{\max} - L_{\min} = L_g \end{cases} \tag{11}$$

where L_g is the length of the grating line.

According to Eq. (11), we get

$$r = \frac{L_g}{2}\sqrt{\frac{4L_{AB}^2 - 4h_{BD}^2 - L_g^2}{4L_{AB}^2 - L_g^2}}. \tag{12}$$

Because the diamond tool begins ruling each grating line when the saddle slider is farthest from point O, we get the expression of diamond tool displacement s as

$$s = L_{\max} - L. \tag{13}$$

Combining Eqs. (11) and (13), we get

$$s = \sqrt{(r + L_{AB})^2 - h_{BD}^2} - r\cos\theta - \sqrt{L_{AB}^2 - (h_{BD} - r\sin\theta)^2}. \tag{14}$$

By assuming that the rotational frequency of the crank is f_0 (Hz) and that the initial phase of the crank is 0, we have

$$\theta = 2\pi f_0 T_s \tag{15}$$

By Eqs. (14) and (15), we get the expression between the diamond tool displacement s and its spent time T_s as

$$s = \sqrt{(r + L_{AB})^2 - h_{BD}^2} - r\cos(2\pi f T_s) - \sqrt{L_{AB}^2 - (h_{BD} - r\sin(2\pi f T_s))^2}. \tag{16}$$

We assume that the grating constant is d and that the original displacement of micro-positioning stage is 0. Assuming no grating ruling error, the displacement of the micro-positioning stage while ruling the kth line should be kd. When we compensate for the line curvature error during ruling, the displacement of the micro-positioning stage during ruling the kth line can be expressed as

$$D(T_s) = kd - E(s) \tag{17}$$

According to Eqs. (9), (10), and (17), after we get the mean line curvature error from the grating diffraction wave fronts of the symmetrical diffraction orders, we can fit the curve of the mean line curvature error and use Eq. (17) to correct the line curvature error by using interferometric control.

4 Experiments

To test our proposed method, we used CIOMP-2 to rule two gratings with a ruling area of ~66 × 8 mm and a line density of 600 line/mm. The diffraction wave fronts of the two gratings were measured by a ZYGO interferometer with a root-mean-squared repetitive error of λ/10,000 and a test wavelength of 632.8 nm.

The first grating was ruled without using our proposed method. Figures 11 and 12 show the +3rd-order and −3rd-

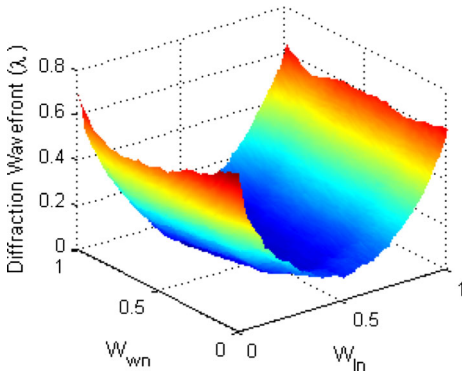

Fig. 11 +3rd-order wave front of the 1st grating

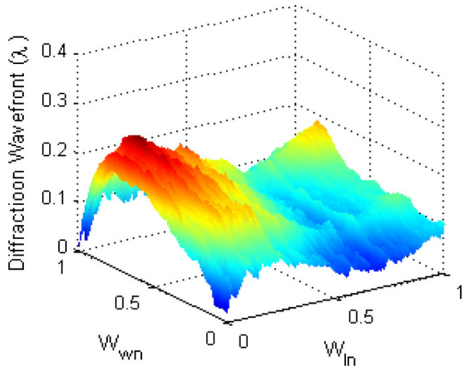

Fig. 12 −3rd-order wave front of the 1st grating

order diffraction wave fronts of the first grating, respectively, revealing the peak-to-valley values of these wave fronts to be $\sim 0.70\lambda$ and $\sim 0.26\lambda$, respectively; W_{ln} is the normalized length of the diffraction wave front, and W_{wn} is the normalized width of the diffraction wave front. We calculated the line error W of the first grating using Eq. (6), as shown in Fig. 13, revealing the peak-to-valley values of the grating ruling error to be ~ 233 nm; G_{ln} is the normalized length of the grating line, and G_{wn} is the normalized width of the grating line. After subtracting the yaw error and the overall position error of each grating line from Eq. (8), we calculated the line curvature error B, as shown in Fig. 14, revealing the peak-to-valley values of the line curvature error B to be ~ 162 nm.

Then, by using Eq. (9) and least-squares fitting, we obtained the mean line curvature error B_m and its curve fit, as shown in Fig. 15, revealing the maximum curve-fitting residual to be ~ 9.7 nm.

To minimize the line curvature error, we used Eq. (17) and integrated interferometric control to adjust the real-time displacement of the stage. A BP-PID control algorithm was used for closed-loop control of the piezoelectric actuators. The second grating was ruled by including our proposed method. Figures 16 and 17 show the +3rd-order and −3rd-order diffraction wave fronts of the second

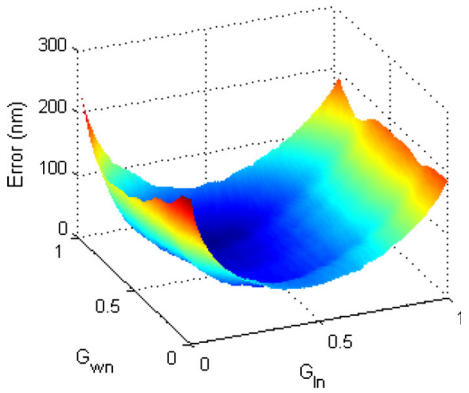

Fig. 13 Line error W of the 1st grating

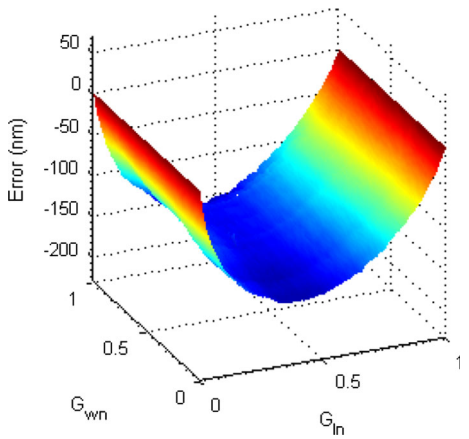

Fig. 14 Line curvature error B of the 1st grating

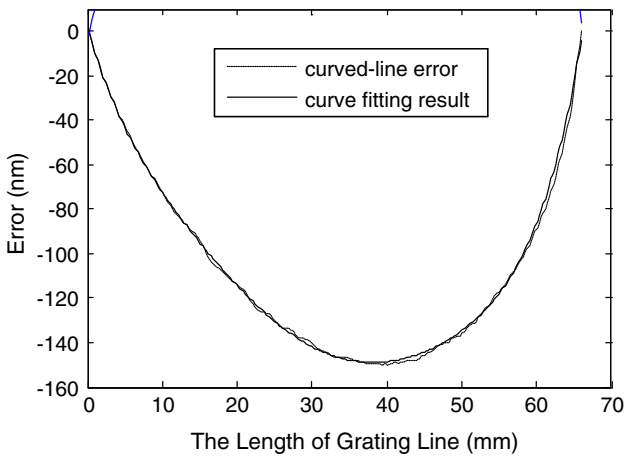

Fig. 15 Mean line curvature error and its fit

grating, revealing the peak-to-valley values of these wave fronts to be $\sim 0.24\lambda$ and $\sim 0.23\lambda$ separately.

Figure 18 shows the line error W of the second grating, revealing the peak-to-valley values of the grating ruling error to be ~ 76 nm. After subtracting yaw error and overall position error of each grating line from Eq. (8), we

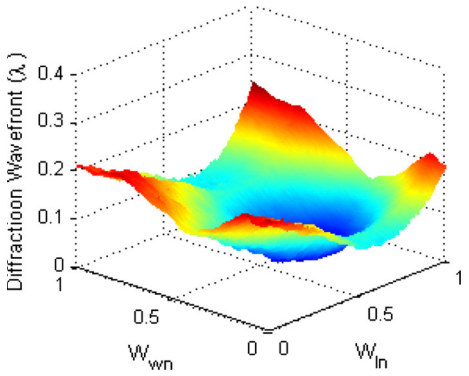

Fig. 16 +3rd-order wave front of the 2nd grating

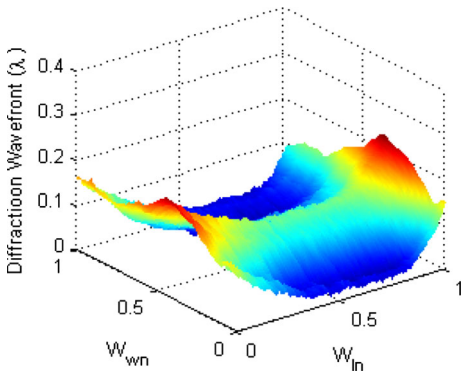

Fig. 17 −3rd-order wave front of the 2nd grating

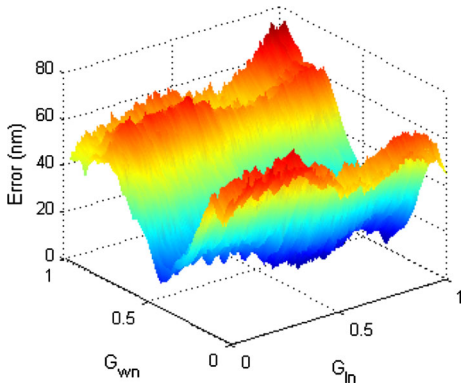

Fig. 18 Line error *W* of the 2nd grating

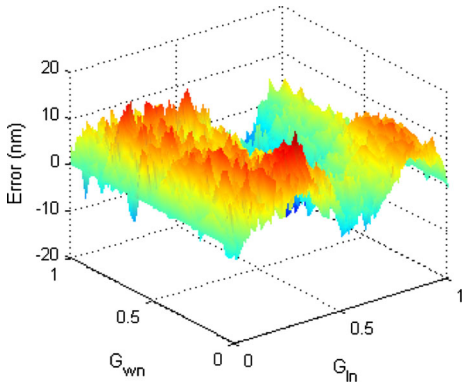

Fig. 19 Line curvature error *B* of the 2nd grating

calculated the line curvature error *B* of the second grating, as shown in Fig. 19, revealing the peak-to-valley values of the line curvature error *B* to be ∼35 nm.

Comparing the first and second gratings, the peak-to-valley values of the line curvature error *B* decreased from 162 nm (see Fig. 14) to 35 nm (see Fig. 19), respectively, showing that our proposed method greatly reduced the line curvature error. By using interferometric control to correct the line curvature error, we also reduced the diffraction wave front of the grating. Comparing the first and second gratings, the peak-to-valley value of the +3rd-order diffraction wave front decreased from 0.70λ (see Fig. 11) to 0.24λ (see Fig. 16), respectively, almost a threefold decrease. However, the −3rd-order diffraction wave front remained almost constant. This behavior occurred because for the 2nd grating, the surface error of grating blank influenced the diffraction wave front much more than did the grating ruling error, and the directions of these two errors are opposite for the −3rd-order diffraction wave front of the 2nd grating.

5 Conclusions

Line curvature error influences the quality of grating diffraction wave fronts. Though this error can be reduced somewhat by changing the mechanical structure of the grating ruling machine, this is inefficient and time-consuming. In this paper, we proposed a method to correct line curvature error by using interferometric control. Our proposed method uses diffraction wave fronts of symmetrical orders to compute the mean line curvature error of the ruled grating and takes the mean line curvature error as the system error. To minimize the line curvature error while the grating is being ruled, we adjusted the real-time displacement of the stage by using interferometric control. To support our method, we provided a detailed mathematical model. Our experiments show that our proposed method reduced the peak-to-valley value of the line curvature error from 162 nm to 35 nm. By using our proposed method, we reduced the influence of the line curvature error on the grating diffraction wave front, improving its quality.

Acknowledgments The authors acknowledge supports from the Chinese Finance Ministry for the National R&D Projects for Key Scientific Instruments (Grant ZDYZ2008-1) and from Ministry of national science and technology for National Key Basic Research Program of China (Grant 2014CB049500).

References

1. G.R. Harrison, S.W. Thompson, H. Kazukonis, J.R. Connell, 750-mm ruling engine producing large gratings and echelles. J. Opt. Soc. Am. **62**(6), 751–756 (1972)
2. F.M. Gerasimov, Use of diffraction gratings for controlling a ruling engine. Appl. Opt. **6**(11), 1861–1864 (1967)
3. T. Jitsuno1, S. Motokoshi et al., Development of 91 cm size gratings and mirrors for LEFX laser system. J. Phys Conf. Ser. **112**, 1–4 (2008)
4. T. Suzuki, H. Kubo et al., High-resolution multi grating spectrometer for high quality deep UV light source production. Proc. SPIE Opt. Microlithogr. XIV **4346**, 1254–1261 (2001)
5. J. Flamand, F. Bonnemason, A. Thevenon, The blazing of holographic gratings using ion-etching. Proc. SPIE **1055**, 288–294 (1989)
6. D. Nevejans, E. Neefs, E. van Ransbeeck et al., Compact high-resolution spaceborne echelle grating spectrometer with acousto-optical tunable filter based order sorting for the infrared domain from 2.2 to 4.3 μm. Appl. Opt. **45**(21), 5191–5206 (2006)
7. K. Takashima, S. Nawata, Diffraction grating ruling engine with piezoelectric control. Jpn. J. Appl. Phys. **17**(8), 1445–1446 (1978)
8. I.R. Bartlett, P.C. Wildy, Diffraction grating ruling engine with piezoelectric drive. Appl. Opt. **14**(1), 1–3 (1975)
9. T. Kita, T. Harada, Ruling engine using a piezoelectric device for large and high-groove density gratings. Appl. Opt. **31**(8), 1399–1406 (1992)
10. J. Strong, The Johns Hopkins University and diffraction gratings. J. Opt. Soc. Am. **50**(12), 1148–1152 (1960)
11. G.R. Harrison, The production of diffraction gratings I. Development of the ruling art. J. Opt. Soc. Am. **39**(6), 413–425 (1949)
12. G.R. Harrison, G.W. Stroke, Interferometric control of grating ruling with continuous carriage advance. J. Opt. Soc. Am. **45**(2), 112–120 (1955)
13. G.R. Harrison, *Techniques for Ruling Improved Large Diffraction Gratings Final Report* (Massachusetts Institute of Technology, Cambridge, 1971), pp. 1–14
14. G.R. Harrison, The diffraction grating—an opinionated appraisal. Appl. Opt. **12**(9), 2039–2048 (1973)
15. X. Li, B. Bayanheshig, X. Qi et al., Influence and revising method of machine-ruling grating line's curve error, location error on plane grating's performance. Chin. J. Lasers **40**(3), 0308009 (2013). (in Chinese)
16. X. Li, Bayanheshig, X. Qi et al., Two-dimensional fast Fourier transform method of analyzing the influence of plane grating's line error and surface error. Acta Opt. Sin. **32**(11), 1105001 (2012). (in Chinese)
17. Z. Jaroszewicz, Interferometric testing of the spacing error of a plane diffraction grating. Opt. Commun. **60**(6), 345–349 (1986)
18. G.R. Harrison, N. Sturgis et al., Interferometrically controlled ruling of ten-inch diffraction gratings. J. Opt. Soc. Am. **49**(3), 205–211 (1959)
19. G.W. Stroke, Attainment of high-resolution gratings by ruling under interferometric control. J. Opt. Soc. Am. **51**(10), 1321–1339 (1961)